E15-2008-94

M. Majerle[1,2], J. Adam[1,3], P. Čaloun[1,3], S. A. Gustov[3],
V. Henzl[1,2], D. Henzlová[1,2], V. G. Kalinnikov[3],
M. I. Krivopustov[3], A. Krása[1,2], F. Křížek[1,2],
A. Kugler[1], I. V. Mirokhin[3], A. A. Solnyshkin[3],
V. M. Tsoupko-Sitnikov[3], V. Wagner[1,2]

SPALLATION EXPERIMENT ON THICK LEAD TARGET:
ANALYSIS OF EXPERIMENTAL DATA
WITH MONTE CARLO CODES

[1] Nuclear Physics Institute of ASCR PRI, 250 68 Řež near Prague, Czech Republic
[2] FNSPE of CTU, 115 19 Prague, Czech Republic
[3] Joint Institute for Nuclear Research, 141980 Dubna, Russia

Майерле М. и др.   E15-2008-94
Реакция скалывания на толстой свинцовой мишени: анализ
экспериментальных результатов с помощью программ Монте-Карло

Программы Монте-Карло MCNPX и FLUKA были использованы для анализа экспериментальных результатов, полученных в декабре 2003 г. в Лаборатории ядерных проблем Объединенного института ядерных исследований (Дубна). Пучок протонов с энергией 660 МэВ направлялся на толстую свинцовую мишень, в которой генерировался поток нейтронов, облучавший небольшие активационные детекторы, располагавшиеся в различных местах мишени. Результаты программ сравнивались с экспериментальными данными и были использованы, в частности, для изучения возникающих в них систематических неопределенностей. Несколько моделей внутриядерного каскада, используемых в программах MCNPX и FLUKA, сравнивались между собой и с экспериментальными результатами.

Работа выполнена в Лаборатории ядерных проблем им. В. П. Джелепова ОИЯИ.

Majerle M. et al.   E15-2008-94
Spallation Experiment on Thick Lead Target: Analysis of Experimental
Data with Monte Carlo Codes

The Monte Carlo codes MCNPX and FLUKA were used to analyze the experiment realized at the Laboratory of Nuclear Problems of the Joint Institute for Nuclear Research (Dubna) in December 2003. A 660 MeV proton beam was directed to a thick lead target producing spallation neutrons, which were probed at different places around the target with small activation detectors. The codes were used to study the systematic uncertainties and to predict the experimental results. Several spallation models included in MCNPX and FLUKA were checked against each other and the experiment. Both codes described successfully most of the experimental results.

The investigation has been performed at the Dzhelepov Laboratory of Nuclear Problems, JINR.

INTRODUCTION

A high power accelerator of middle energy (few 100 MeV) coupled with a spallation target offers an alternative method of producing neutrons, useful in research or for energy production and nuclear waste transmutation in accelerator driven systems (ADS). The theoretical descriptions of processes in the target exist for many decades, however, extensive experimental tests are showing that our knowledge of them is not complete. Numerous spallation experiments were performed so far and checked against the calculations based on theoretical models. Most of such experiments are focused either on the number of produced neutrons per one proton (the spallation target is enveloped with the moderator and the fluence of thermal neutrons outside the moderator is measured) [1], or on angular and energy distributions of spallation neutrons (a thin spallation source is surrounded with neutron detectors at different angles) [2]. There is no experimental data about the energy spectrum of produced neutrons in the first case. In the second case, only spallation is studied without any subsequent processes.

Monte Carlo codes such as MCNPX [3] and FLUKA [4] are quite successful in the prediction of the results of such experiments — the differences between the predictions and the experiments are usually less than 50%. Moreover, various spallation models included in codes agree with the experiments on the total number of produced neutrons within only few percents, differences arise with the predictions of the spectra of neutrons with energies higher than 10 MeV, which represent around one tenth of all produced neutrons.

The codes have the key role at the estimation of the systematic uncertainties of such experiments. The experimental parameters are always controlled with finite accuracy, and by changing the parameters within these limits in simulations, their impact on the results can be studied.

It is expected that the codes would describe more complicated setups less accurately than simple experiments — the measured quantities are the averages from multiple processes (spallations, transport) and the inaccuracies of the description of single processes are summed. However, many experiments with simplified ADS setups performed so far at the Joint Institute for Nuclear Research (Dubna) were used to check various simulation codes [5], and the disagreements are in general within 50%.

1

The data from one of the latest JINR experiments are presented in this paper. At the experiment, relativistic protons were directed to a thick lead target and produced neutrons were probed with activation detectors. Neutron spectrum was not modified with moderators and the results from activation detectors, used for their small size and the capability to probe the neutron spectrum in the energy range 10–100 MeV, are very useful for the valuation of different spallation models exactly in the energy range of large disagreements between them.

1. THE EXPERIMENTAL SETUP AND RESULTS

1.1. Experimental Setup. The setup consisted of a cylindrical lead target with the radius of 4.8 cm and length of 45.2 cm, placed at the end of the concrete corridor with length of 20 m, height and width of 2 m and 2 m thick walls (Fig. 1). The target was separated in two cylindrical parts (with lengths of 12.3 cm and 32.9 cm) and 0.7 cm air gap between them. Both parts were made of smaller segments (in cm: 4.7; 3.8; 3.8; gap 0.7; 3.3; 4.6; 4.3; 4.2; 3.9; 4.8; 3.8; 4).
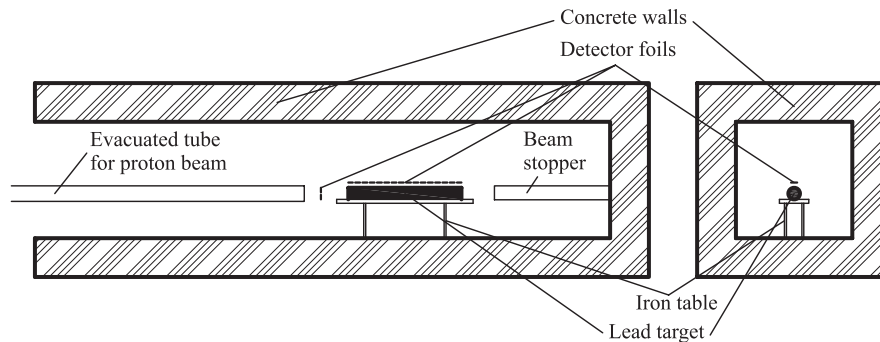

Fig. 1. The layout of the Phasotron experimental setup. Longitudinal (left) and transverse (right) cross sections

Activation detectors, made of Al, Au, and Bi thin foils (dimensions 2 cm × 2 cm × 0.05 mm for Al and Au foils and 2.5 cm × 2.5 cm × 1 mm for Bi foils) were placed on top of the setup along its whole length. Au and Al detectors were placed every 2 cm from the beginning of the target and Bi detectors were placed on the 1st, 9th, 21st, 31st, and 43rd cm. Five sets of Al and Au activation detectors were placed in the gap, one detector set on the target central axis and four sets around it, forming a cross with ca. 3.5 mm space between the foils, as seen in

2

Fig. 2, a^*. In front of the target were placed detectors for the measurement of the beam integral made of bigger Al and Cu foils (8 cm × 8 cm × 0.1 mm).

High energy neutrons produced during the irradiation were at the same time used for the studies of transmutation of radioactive isotope iodine ^{129}I. Four iodine samples were placed on top of the setup, two samples at 9th cm and other two samples at 21st cm. Each pair of the samples contained a sample with natural iodine (^{127}I) and another with iodine from the nuclear waste (mixture of 17% ^{127}I and 83% ^{129}I) in the form of NaI. ^{127}I samples were in the form of solid cylindrical tablets ($r = 1.05$ cm, $h = 0.3$ cm), and ^{129}I samples were prepared from NaI powder packed in Al shielding [6]**.
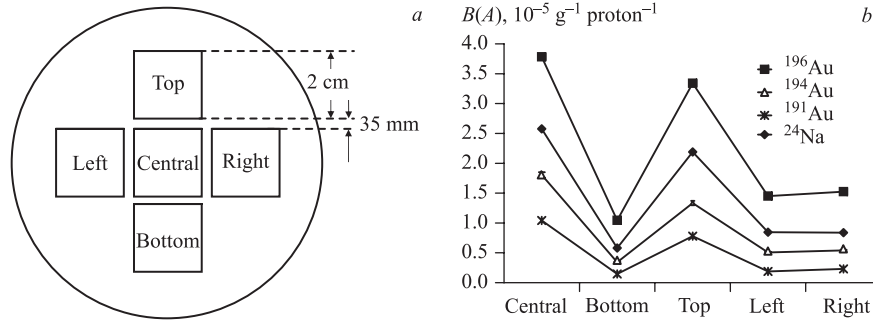

Fig. 2. The placement of the five sets of Al and Au detectors in the gap (a) and production rates (b) for ^{24}Na in Al foils and ^{191,194,196}Au in Au foils (statistical errors are not seen at this scale)

After 10 minutes of irradiation with the proton beam of approximate intensity (10^{13} protons/s), the detectors and samples were collected from the setup. Their gamma spectra were measured with HPGe spectrometers. The detectors were measured twice, soon after the irradiation for a short time, and after the decay of short living isotopes for a longer time. The iodine samples were measured ≈ 10 times. Gamma spectra of radioisotopes with decay times from few minutes up to some days were registered. The spectra were analyzed using the standard method (described in [7]) and the amount of activated/transmuted material in the detectors was determined. The quantity introduced as the production rate $B(A)$ —

---

*Shortly before the experiment, these foils were manipulated and it is possible that they were not centered after that.

**The aluminum shielding was remodeled for this experiment to provide reasonable safety at the minimum of Al used.

the mass of activated isotope A per one incident proton and per 1 g of detector material — is used to present the results.

1.2. Experimental Data — Beam Parameters. During the irradiation, the beam was monitored with the wire chamber placed at the end of the beam tube. The wire chamber showed that after ten minutes of constant irradiation, the beam centered to the central target axis, with the intensity of ca. 10^{13} protons/s and with horizontal and vertical diameters of 1.6–1.9 cm was produced.

Independently, the beam integral was measured with the activation detectors, big Al and Cu foils, placed in front of the target. Their analysis showed that isotopes ^{24}Na (not used for the determination of the beam integral, part of it is produced by neutrons) and ^{7}Be are found in Al foil and ^{7}Be, ^{24}Na, ^{42}K, ^{43}K, ^{44}Sc, ^{44m}Sc, ^{46}Sc, ^{47}Sc, ^{48}Sc, ^{48}V, ^{51}Cr, ^{52}Fe, ^{52}Mn, ^{54}Mn, ^{55}Co, ^{56}Co, ^{57}Co, ^{58}Co, ^{57}Ni in $^{\mathrm{nat}}$Cu foil. From the production rates and the cross sections for this isotopes (taken from EXFOR [8] and extrapolated to 660 MeV if necessary) the number of protons was calculated. Mean weighted average value of the integral proton flux was determined to be $1.58 \cdot 10^{15}$ protons with the accuracy of 6%.

The beam diameter and displacement from the central axis were measured with the cross of five sets of Al and Au detector sets placed in the gap between the target sections. The production rates are shown in Fig. 2, *b*. Comparing the rates in different foils, one can conclude that the beam had the elliptical shape (the ratio between the horizontal and vertical axis was 0.6:1) and that the center of the beam was somewhere between the central and the top foils. Shortly before the experiment the cross with the detectors was manipulated and it is possible that it was displaced from the target center.

1.3. Experimental Data — Longitudinal Neutron Field. In the detectors used for the measurement of longitudinal distribution of high energy neutrons were found the following isotopes: in Al detectors ^{24}Na, in Au detectors ^{189}Au–^{196}Au, ^{198}Au and in Bi detectors ^{201}Bi–^{206}Bi. The production rates against the position along the target are plotted in Fig. 3, *a, b, c* for all three types of detector foils. The error bars are only statistical uncertainties of the gamma peak approximation with Gaussian curve.

The graphs show the specific shape: the maximum at around the 8$^{\text{th}}$ cm, and the point near the 30$^{\text{th}}$ cm, where the neutron field starts to decrease faster. The second point coincides with the range of 660 MeV protons in lead — protons with such energy are stopped due to ionization losses after 31 cm of lead material according to calculation (Fig. 3, *d*) [9]. After ca. 30 cm of the lead, there is no more spallation by primary particles, what is seen as a fast decrease of production rates after this point. The graph for ^{198}Au, which is produced through (n, γ) reaction channel by low-energy neutrons shows constant production along the target. The neutrons from the target were moderated and partly reflected back by concrete walls, resulting in almost homogeneous low-energy neutron field around the target, which is seen as a flat distribution of production rates of ^{198}Au.
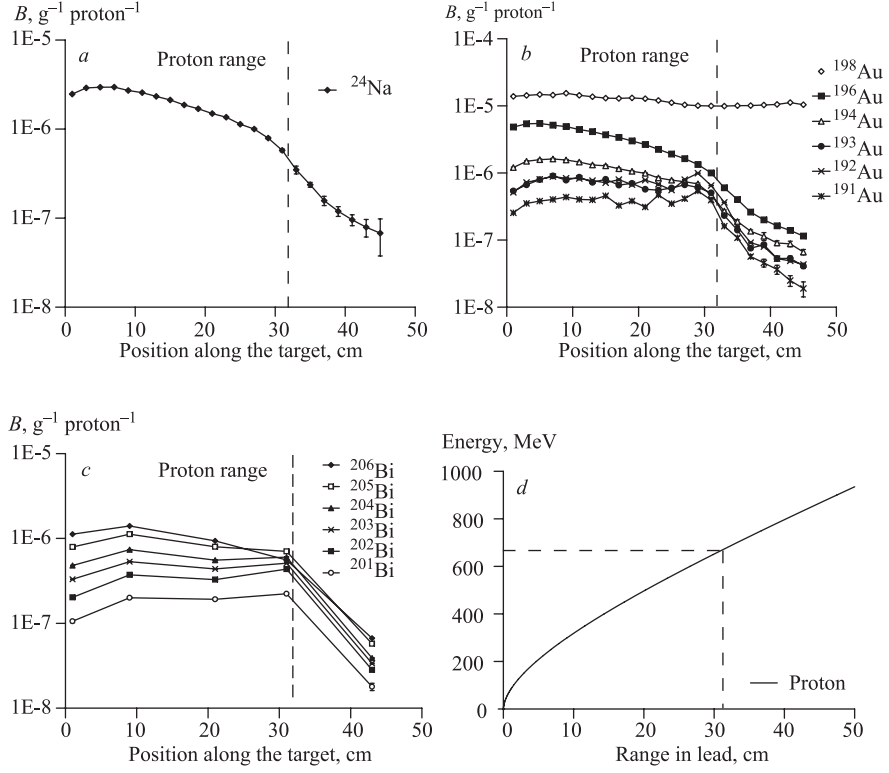
4

Fig. 3. B-values for ^{24}Na in Al foils (a) and different isotopes in Au (b) and Bi (c) foils along the target (errors at the graphs are only statistical errors). In (d) is shown the proton range in lead depending on the energy [9]

1.4. Experimental Data — Transmutation of Iodine. The main interest in the experiment was to measure the production rates of higher order reactions in iodine — $(n, 5n)$, $(n, 6n)$,... reactions. Actually, the yields of produced isotopes up to ^{118}I — $(n, 10n)$ — were determined with the accuracy of 10%, and the products decayed from iodine isotopes up to ^{116}I — $(n, 12n)$ — were detected. The yields of produced isotopes for ^{129}I were calculated with the substraction of ^{127}I contribution in the samples with the mixture of radioactive and stable iodine.

The graphs in Fig. 4 show the production rates of measured iodine isotopes at the 9th cm and the 21st cm for ^{127}I and ^{129}I. The production rates lie in the range between 10^{-8} g^{-1}proton^{-1} and 10^{-5} g^{-1}proton^{-1}.
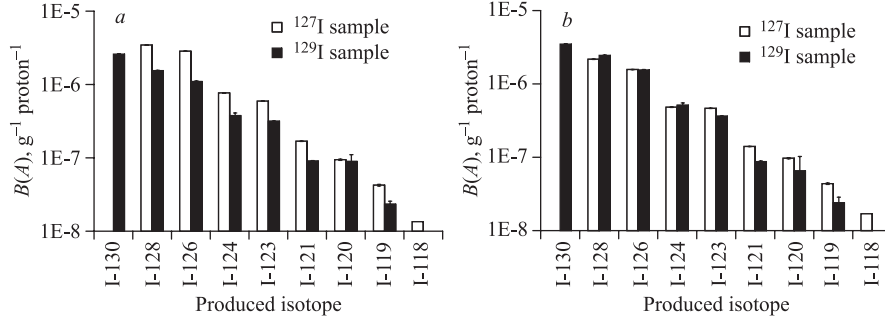
5

Fig. 4. B-values for different isotopes in ^{127}I and ^{129}I. Samples were placed at the 9th (a) and 21st cm (b)

2. SIMULATIONS — SYSTEMATIC UNCERTAINTIES OF EXPERIMENTAL RESULTS

The experimental setup was simulated using the MCNPX v2.6.0f code package [10] and the FLUKA [4] code. In the simulations, the target was approximated with the lead cylinder with its real dimensions and the concrete with 2 m thick walls. The beam tube, the beam stopper and the table on which the setup was placed were approximated with an evacuated iron tube ($r = 10$ cm, $d = 0.5$ cm, ends 30 cm before the target), full iron tube ($r = 10$ cm, starts 55 cm after the target) and iron plate (1 cm thick, 1 m × 0.5 m), respectively. The detectors were approximated with thin foils with realistic dimensions and the samples were approximated with realistic thin cylinders (enveloped in aluminum shielding — ^{129}I samples).

In the simulations with the MCNPX code package two cascade models (CEM03 [11], INCL4/ABLA [12, 13]) and LA150 [14] libraries were used. In FLUKA, the preequilibrium-cascade model PEANUT [15] and FLUKA's own cross section libraries (for materials used at this experiments imported from ENDF/B-VI) were used.

Neutron and proton fluences in the detectors and iodine samples binned in 1 MeV energy intervals (1–150 MeV, 50 MeV bins above 150 MeV) were calculated. These fluences were convoluted with the (n, xn) cross sections calculated with the TALYS-1.0 [16] code (and MCNPX code using CEM03 model for energies higher than 150 MeV) in order to obtain the production rates $B(A)$.

2.1. The Influence of the Setup Parts and Experimental Uncertainties to the Results. At the first step, the MCNPX (CEM03 cascade model) simulation was done with the thin central beam and the obtained results were compared

to the experimental measured values. Most experimental values were described well, with the two points mentioned in Subsec. 1.3 (maximum at 10th cm and faster decrease of production rates after 30th cm) at the right places, and with the differences between experimental and simulated production rates which were within 30%.

At the next step, a set of MCNPX simulations with changed setup parameters was performed in order to study the influence of the setup parts such as concrete walls and iron componets on the experimental results, and to estimate the systematic uncertainty of the experimental results (mainly becasue of the beam parameters).

2.1.1. Concrete walls and iron parts. Concrete walls moderate neutrons coming from the target and reflect part of moderated neutrons back to the setup place, thus they produce an almost homogeneous field of low-energy neutrons
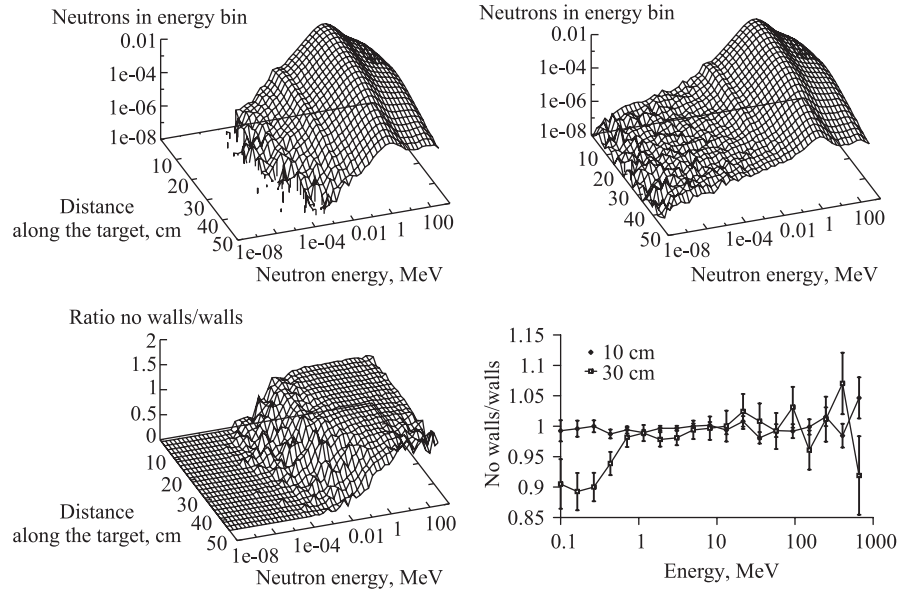

Fig. 5. The neutron spectra along the target length calculated with MCNPX CEM03. The left upper figure shows the case without the concrete and the right upper figure shows the case, where concrete walls moderated fast neutrons and reflected part of them back to the setup creating almost homogeneous low energy neutron background. On the lower figures are plotted the ratios between the calculated spectra for the setup without and with concrete walls. On the left are the ratios for the whole energy spectrum along the target, and on the right are shown the ratios between spectra at energies 0.1–660 MeV at positions 10 and 30 cm from the beginning of the target. Concrete walls have no influence on the neutron spectra in the energy range 1–660 MeV

7

around the target. Calculated neutron spectra along the target for the case with the walls included and for the case without walls are seen in Fig. 5 together with the ratios between them. It is important to stress that the high energy part of the produced neutron spectrum is not changed due to the walls (the ratio between the spectra is 1 within the error bars), there is no physical mechanism how high-energy neutrons could be reflected back to the setup. The same conclusion applies also to protons. Calculations of production rates of threshold reactions for the setup with and without walls confirmed that the results do not differ outside the statistical uncertainties which were 2%. One can conclude that the walls have no influence on high energy neutron field (and on production rates in threshold detectors). However, they change significantly the neutron field for neutrons with energies < 100 keV, neutrons scattered from the wall contribute from 20–90% to the production rates of ^{198}Au (at the beginning and at the end of the target, respectively), as is seen in Fig. 6.

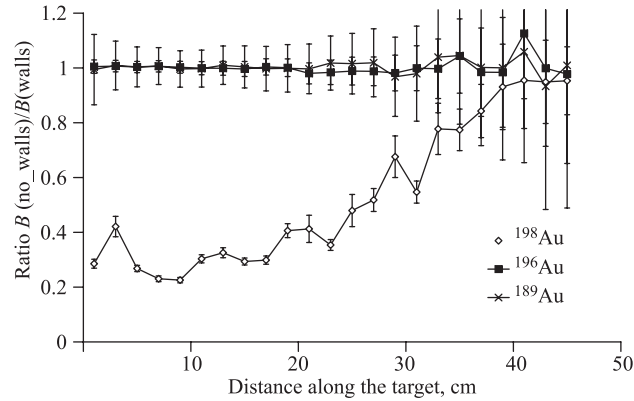Fig. 6. The ratios of the production rates of ^{198}Au, ^{196}Au and ^{189}Au along the target calculated with MCNPX for the cases with and without concrete walls. ^{198}Au is produced from 20–90% by the moderated neutrons from the concrete walls, but $^{196-189}$Au are produced only by neutrons from the target, concrete walls have no influence on their production rates

In the iron parts of the setup, a mechanism that could change the high energy neutron field exists. Heavy Fe nuclei can scatter neutrons, and additionally, in spallations or (n, xn) reactions in iron, more neutrons can be produced. Calculations were performed to estimate the importance of these effects. A simulation was performed with the iron parts approximated as described in the introduction of Sec. 2, and another one — where iron parts were replaced with air. It was found out that iron parts have negligible influence on threshold and (n, γ) reactions. With the iron parts included, the reaction rates after 30th cm are 5% lower than without iron (statistical uncertainties are 5%).

8

2.1.2. Beam parameters. Several simulations with miscentered beams and different beam profiles were compared. The beam was at first approximated with a point beam, directed to the center of the target. In the following five simulations, the beam was displaced every time for 0.3 cm upwards. This direction should have the biggest influence on the results — it is the direction towards the detectors placed on top of the target. In the detectors on top of the setup and iodine samples the increase in production rates for nonthreshold reaction (n, γ) was 10% for each displacement. For the threshold reactions, the increase at every displacement was 10 and 15% for $(n, 2n)$ and $(n, 10n)$ reactions, respectively. The differences are significant only up to the 30th cm, with the range of the proton beam.

Then another direction of the displacement was chosen, the beam was displaced to the left. It was found out, that displacement to the left has much lower influence on the results: the displacement of the beam for 1.5 cm lowered the production rates (threshold and nonthreshold reactions) for less than 10%.

Finally, the calculations with the beam approximated with the Gaussian profile with FWHM = 2 cm and FWHM = 4 cm were compared to the first simulation with the point beam. The reaction rates increased with the width of the beam. For the beam with FWHM = 4 cm, the icrease is 15 and 40% for $(n, 2n)$ and $(n, 10n)$ reactions, respectively. The changes are significant only in the detectors at the beginning of the target, after the 10th cm, the changes are much smaller. For the beam with the FWHM = 2 cm (the experimental beam had smaller FWHM than 2 cm), no changes were observed from the point beam. The beams with the cylindrical shape behave similarly as those with the Gaussian profile.

As the profile and horizontal displacements of the beam do not influence the experimental results significantly, the only source of systematic uncertainty is the beam displacement on the vertical axis. The accuracy of the beam position was 3–4 mm that brings 15% systematic uncertainty in the experimental results of the top detectors and iodine samples.

2.1.3. Detectors and samples displacement. The calculation with the detectors displaced to the left for 0.3 cm was performed. The reaction rates did not differ from the reaction rates for not displaced detectors within the limits of statistical uncertainties (5%). The displacement of the detectors upwards for 2 mm produces for ca. 5% lower reaction rates in detectors at the beginning of the target, the difference decreases to 0 around the 20th cm.

Another calculation with the detectors displaced for 0.3 cm along the target showed that in the detectors placed far from the 30th cm, the reaction rates are not sensible to such a displacement. For the isotopes produced through (n, xn) and $(p, (x-1)np)$ reactions with $x > 4$, there is another peak in production rates around the 30th cm, see Fig. 7. It is caused by primary protons, which are deviated from their initial direction by Coulomb interactions and reach the target surface around this point. They contribute up to 50% to the production of isotopes from higher (n, xn) reaction. The peak maximum moves to the neighbor detector if

9

detectors are displaced along the target for 0.3 cm. This is also observed if the target is simulated with extra 0.5 mm air gaps inserted between the segments. The production rates in the peak change for 50% when detectors are displaced along the target or the target is extended with gaps between segments comparing with the normal setup.

Apart from the foils near the 30th cm, the detectors are not sensible to small displacements along the target. The detectors and target positions are known with the accuracy ca. 1 mm, the systematic uncertainty is below 5%.

Similar calculations were performed for iodine samples. The accuracy of placement of these samples was not so good and 0.5 cm displacement along the target or in the upward direction is possible. The systematic uncertainty of the experimental results in the iodine samples was calculated to be 30%.

2.1.4. Proton and pion induced reactions. Part of the radioactive material in the detectors is produced by protons and pions (only in threshold reactions). The calculations showed that the production of radioisotopes in reactions with
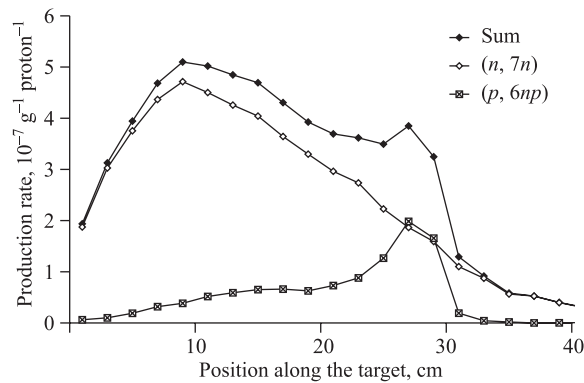

Fig. 7. The production rates for $^{197}\mathrm{Au}(n,7n)^{191}\mathrm{Au}$ and $^{197}\mathrm{Au}(p,6np)^{191}\mathrm{Au}$ reactions (and their sum) along the target calculated with MCNPX. Around the 30th cm, the protons contribute 50 % to the total production rate. Scale on Y axis is linear, so that the second peak is better seen. Statistical errors (ca. 15 %) are not shown on the graph

pions is at least three orders of magnitude lower than the production in reactions with neutrons and thus negligible. Protons influence mainly the production rates of (n,xn) reactions with higher x, and their influence is the biggest around the 30th cm of the target (the point of rapid decrease of the neutron field). At that point their contribution to the total production rate was 10% for $(n,2n)$, 40% for $(n,6n)$, and 50% for $(n,9n)$ reactions, see Fig. 7.

10

3. SIMULATIONS — COMPARISON OF CODE PREDICTIONS WITH EXPERIMENTAL RESULTS

3.1. Determination of the Beam Parameters by Simulations. The exact conclusions about the beam shape and position were not possible from the experimental data. Few MCNPX simulations (CEM03 cascade model) with different beams were performed to find the approximation of the beam, that would produce the reaction rates in the monitor foils and in the top foils close to the experimental ones.

The beam data from the cross of monitor foils suggested that the beam was displaced upwards, so that the center is somewhere between the central and the top foil, and that the beam FWHM is 0.7 and 0.8 cm in the X and Y direction. Such a beam describes the reaction rates in the monitors well, but predicts 1.6 times higher values in the top detectors (Fig. 8).
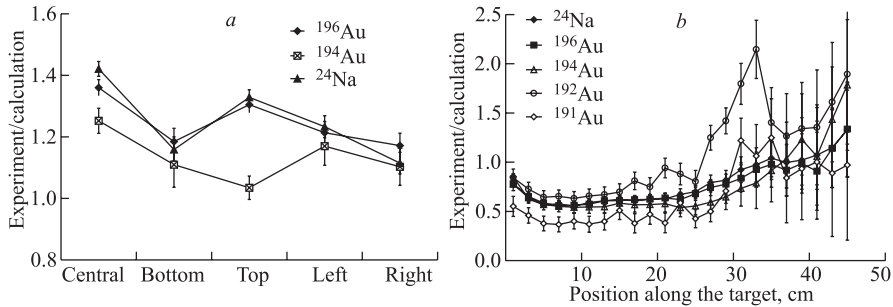

Fig. 8. a) Ratios between experimental and simulated B-values in beam monitor foils placed in the gap. The beam in this simulation was approximated with the Gaussian profile with FWHM in the X and Y direction of 0.7 and 0.8 cm and displaced for 1.1 cm upwards and 0.1 cm to the right. b) Ratios between experimental and simulated B-values in Au and Al detectors placed along the target. INCL4/ABLA models were used to simulate B-values

Obviously, the beam was not displaced upwards (also the data from the wire chamber show that the beam was centered to the target axis). The simulation with the centered beam (FWHM in the X and Y direction were 0.7 and 0.8 cm) predicts the values in the top detectors well. It predicts well also the values in the cross of the monitor detectors, assuming that the cross was displaced downwards for 0.5–1 cm.

The conclusion about the exact beam position could not be made, because the data from the wire chamber and from the cross of monitor detectors do not agree. From the simulations and the experimental data we assume that the beam

was centered, but its position uncertainty is ca. 3 mm. The simulations from this section concerning the beam parameters showed that the systematic uncertainty of the experimental results on the top of the target is therefore 15%.

3.2. Simulations of Neutron Fluences in Detectors on Top of the Setup.

3.2.1. Simulations with CEM03 cascade model. The complete setup was then simulated with the beam parameters which were determined above. The calculations were successful in describing the spatial distributions and the absolute values of production rates along the target.
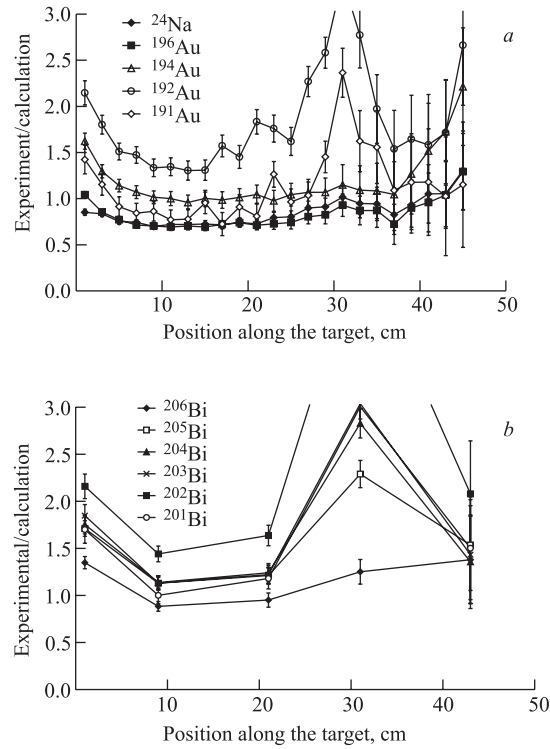

Fig. 9. Ratios between experimental and simulated B-values in Au, Al (a), and Bi (b) detectors placed along the target. CEM03 cascade/evaporation was used to simulate B-values

The distribution of low-energy neutrons along the target which was calculated predicts an almost homogeneous distribution (as the experiment), but experimental values for ^{198}Au are ca. 1.5 higher than calculated production rates. However, the experiment was not focused on low-energy neutrons, the structure details about concrete walls were not known accurately, and this underestimation is explained with the material and geometry uncertainties of concrete walls which influence low-energy neutrons significantly, see Fig. 6.

The calculated production rates of threshold reactions (high-energy neutrons) describe the experiment well: there is a maximum at around 8th cm, and near the 30th cm the values start to decrease faster. The absolute values are described well except for some isotopes (^{191}Au, ^{202}Bi), see Fig. 9.

A sharp peak for some isotopes ($^{191-192}$Au, $^{202-205}$Bi) in experimental/calculation ratios around the 30st cm is also visible in the graph. This is the point, where the protons exit the target material and produce radioactive isotopes in the detectors and the peak can be explained with the systematic uncertainties of the experimental data (see Subsec. 3.1). The results around this point are very sensitive to two parameters of the setup that could not be controlled enough precisely: the displacement of the detectors along the target (uncertainty 1–2 mm) and small gaps between the target segments (1 mm). The additional simulation with extra 1 mm gaps between the target segments showed that the peak is reduced while the other ratios stay unchanged.

3.2.2. Simulations with INCL4/ABLA cascade model and FLUKA code. Simulations were repeated using the INCL4/ABLA model from MCNPX code package.
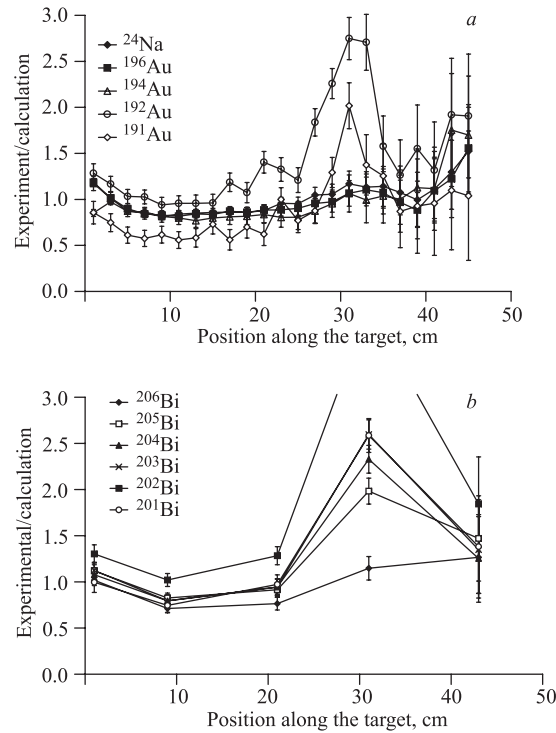

Fig. 10. Ratios between experimental and simulated B-values in Au and Al detectors (a), and in Bi detectors (b). INCL4/ABLA models were used to simulate B-values

13

The comparison between the experimental and calculated values in the beam monitor and detectors on top of the setup are shown in Fig. 10. INCL4/ABLA predicts similar results as CEM03, with some ratios closer to 1 and with a bit decreased peak around the 30th cm. It is worth noting that both simulations predict similar ratios for isotopes ^{196}Au and ^{24}Na, but disagree in the ratios of isotopes with higher thresholds ($^{191-192}$Au, Bi).

Using the same setup approximations as for the MCNPX simulations the neutron and proton fluences were calculated with the FLUKA 2006.3b code. The numbers of neutrons/protons were convoluted with the same cross sections as for MCNPX simulations.

In Fig. 11 it is seen that the ratios for different isotopes in FLUKA calculation are closer to 1 than in MCNPX calculations and also that the peak around the 30th cm is reduced. Only in the detectors at the beginning of the target, experimental values are significantly higher than FLUKA prediction.
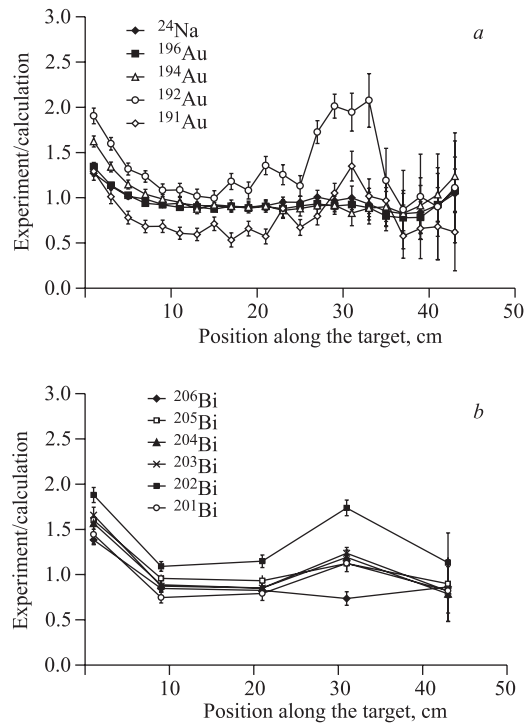

Fig. 11. Ratios between experimental and simulated B-values in Au and Al detectors (a), and in Bi detectors (b). FLUKA 2006.3b code was used to simulate B-values

14

3.2.3. Comparison between codes/models. The neutron and proton spectra in the detector foils on top of the setup were calculated with MCNPX models CEM03 and INCL4/ABLA and with the FLUKA code and were compared with each other. In Fig. 12 are compared the neutron spectra in the detector foil at the 9th cm. The biggest disagreement between spectra is in the energy region below 3
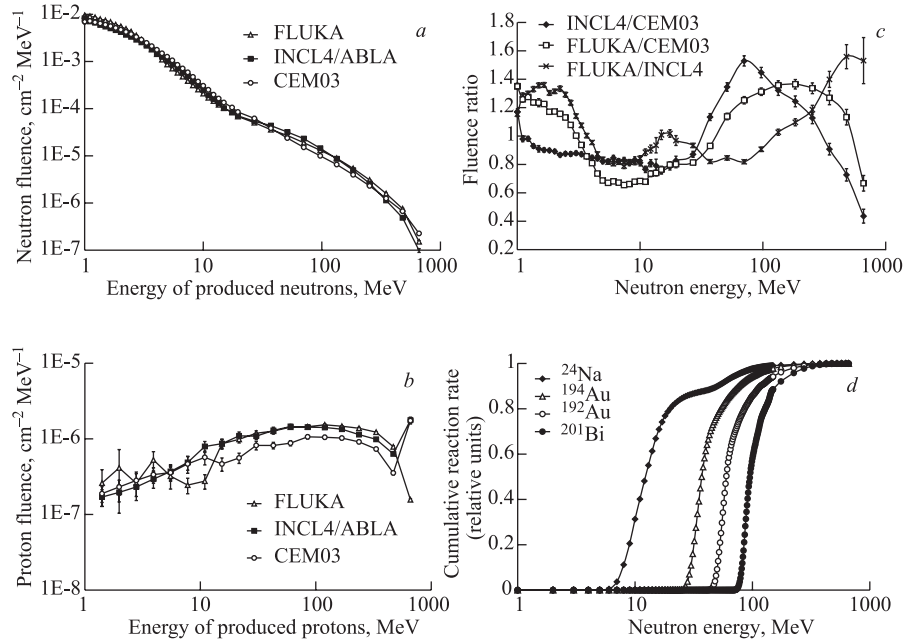

Fig. 12. The neutron (*a*) and proton (*b*) spectra in the detector foil on the 9th cm calculated with the MCNPX CEM03, MCNPX INCL4/ABLA and the FLUKA code, and the ratios between the calculated neutron spectra (*c*). In (*d*) are the cumulative reaction rates (in relative units, normalized to 1) calculated with MCNPX CEM03. It can be seen that ^{24}Na, ^{194}Au, ^{192}Au and ^{201}Bi are produced mainly with 10, 30, 60 and 90 MeV neutrons, respectively

and above 30 MeV and is up to 50%. This disagreement is observed in different predictions of high threshold reaction rates by different codes (e.g., ^{191}Au in Figs. 9, 10, 11). The neutrons with energies above 30 MeV present less than 10% of all produced neutrons. Concerning the total number of produced neutrons per one incident proton, the codes are in good agreement. The FLUKA code and MCNPX INCL4/ABLA predict values of 11.8 and 11.7 produced neutrons per one primary proton and MCNPX CEM03 predicts slightly higher value of 12.6 produced neutrons per one primary proton.

15

3.3. Simulations of Neutron Fluences in Iodine Samples. The neutron and proton fluences in iodine samples were calculated with the MCNPX code package using the INCL4/ABLA models. The fluences were convoluted with cross sections which were also calculated with TALYS/MCNPX. In Fig. 13 are shown the ratios
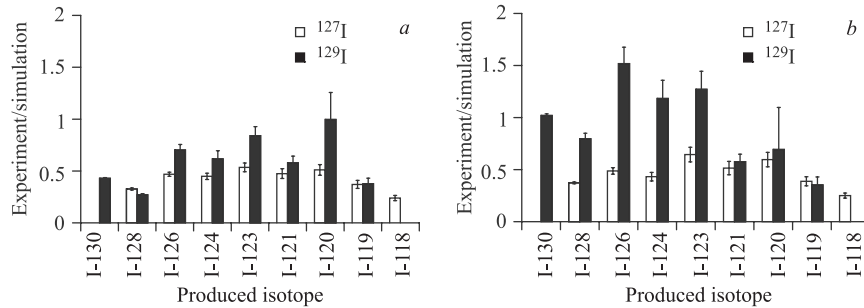

Fig. 13. Ratios between experimental and simulated B-values for different isotopes in ^{127}I and ^{129}I. Samples were placed at 9th (a) and 21st cm (b). INCL4/ABLA was used to simulate B-values

between the experimental and simulated production rates in iodine samples. In a rude approximation, one can see that MCNPX overpredicts the production rates. It must also be noted that the systematical uncertainties of the experimental data in the samples was close to 50% because of the samples and beam position uncertainty. The simulations with other models and with the FLUKA code predict similar results.

CONCLUSION

The Phasotron experiment with a thick bare lead target provided a large set of experimental data (see Tables 1, 2, 3), useful for the benchmark of the Monte Carlo codes. Neutrons, produced at the irradiation of the target with relativistic protons, were probed with many small activation detectors, which provided information about high- and low-energy neutrons. The focus of the experiment was on the production of neutrons with energies higher than 10 MeV (representing one tenth of all produced neutrons), the energy region where the predictions of the various Monte Carlo codes are not yet accurate. The parameters of the setup were not appropriate for the measurements of the low energy part of the produced neutron spectrum and the results concerning low-energy neutrons are useless for benchmark tests.

The simulation procedure was based on convolution of the calculated neutron and proton spectra with the pre-computed cross sections (TALYS code). With the comparison of the simulation results (setups with changed parameters were

Table 1. Experimental reaction rates in Au foils along the target. X **(cm) is the distance of the foil center from the beginning of the target. Reaction rates** $B(A)$ **are multiplied with** 10^8

X, cm	^{198}Au	^{196}Au	^{194}Au	^{193}Au	^{192}Au	^{191}Au
1	1385 ± 5	483.3 ± 2.8	120.5 ± 2.2	53.9 ± 1.0	51.4 ± 0.6	24.7 ± 0.7
3	1432 ± 8	540 ± 3	149 ± 3	66.6 ± 1.1	72.2 ± 0.9	34.5 ± 0.8
5	1476 ± 10	547 ± 5	158 ± 3	79.5 ± 1.2	80.4 ± 1.1	37.0 ± 1.1
7	1447 ± 15	515 ± 8	161 ± 4	90.4 ± 1.3	88.4 ± 1.1	39.6 ± 1.3
9	1543 ± 6	490.9 ± 2.1	156 ± 2.6	78.0 ± 1.0	83.4 ± 2.0	43.2 ± 1.4
11	1435 ± 16	444 ± 7	145 ± 4	86.3 ± 1.5	82.6 ± 0.9	39.1 ± 1.0
13	1367 ± 9	413 ± 3	131.6 ± 2.8	72.5 ± 1.1	76.9 ± 0.9	39.1 ± 1.2
15	1304 ± 13	370 ± 3	128 ± 4	80.4 ± 1.4	71.4 ± 0.6	45.2 ± 1.3
17	1290 ± 9	338.7 ± 1.9	116 ± 3	65.9 ± 1.1	79.6 ± 1.4	32.0 ± 1.1
19	1314 ± 9	300 ± 4	105.9 ± 2.8	70.0 ± 1.3	66.9 ± 0.6	37.4 ± 1.3
21	1278 ± 7	265.4 ± 1.6	98.8 ± 1.9	57.2 ± 0.9	78.2 ± 0.7	30.4 ± 0.8
23	1203 ± 12	224.4 ± 3	84 ± 3	55.4 ± 1.1	67.9 ± 1.8	46.1 ± 1.4
25	1114 ± 7	191.1 ± 1.7	78 ± 2.2	59.6 ± 1.1	55.6 ± 1.2	34.0 ± 0.8
27	1035 ± 8	163.1 ± 1.8	74 ± 2.6	66.6 ± 1.5	79.5 ± 0.7	40.8 ± 1.9
29	1010 ± 10	133.6 ± 0.9	68.6 ± 2	60.9 ± 1.3	99.2 ± 1.1	51.4 ± 1.3
31	996 ± 11	99.9 ± 1.2	47 ± 2.3	50.6 ± 0.8	64.9 ± 0.7	38.8 ± 1.3
33	990 ± 10	60.1 ± 0.4	27 ± 1.1	23.2 ± 0.4	36.4 ± 0.4	15.6 ± 0.4
35	1007 ± 6	40.1 ± 0.4	18.9 ± 1.1	14.1 ± 0.4	15.78 ± 0.23	10.7 ± 0.6
37	1011 ± 5	26.1 ± 0.3	13.5 ± 0.7	7.6 ± 0.4	9.15 ± 0.13	5.4 ± 0.3
39	1030 ± 4	20.0 ± 0.4	11.4 ± 1.6	8.5 ± 0.6	7.98 ± 0.19	4.5 ± 0.6
41	1051 ± 3	16.3 ± 0.4	9 ± 0.7	5.3 ± 0.4	5.3 ± 0.3	3.6 ± 0.6
43	1119 ± 3	13.9 ± 0.5	8.8 ± 0.8	5.3 ± 0.4	4.90 ± 0.16	2.5 ± 0.4
45	1039.8 ± 2.9	11.5 ± 0.4	6.6 ± 0.6	4.1 ± 0.3	4.32 ± 0.14	1.9 ± 0.5

simulated using MCNPX) it was found out that the systematic experimental errors are 15%, with the exception of few particular detectors (detectors around the 30th cm). The biggest systematic uncertainty arises with the uncertainties in the beam position, which should threfore be controlled with most attention. Unfortunately, the additional monitor detectors in this experiment were obviously misplaced, what caused the mentioned systematic uncertainty. However, reliable data on high energy neutron and proton production and transport were obtained. The results concerning the transmutation properties of ^{129}I in high-energy neutron field are less accurate, because of geometrical and material uncertainties of the samples.

The benchmark tests with several cascade/evaporation models included in the MCNPX code package and with the FLUKA code showed consistent results.

Table 2. Experimental reaction rates in Al and Bi foils along the target. X (cm) is the distance of the foil center from the beginning of the target. Reaction rates $B(A)$ are multiplied with 10^8

X, cm	^{24}Na	^{206}Bi	^{205}Bi	^{204}Bi	^{203}Bi	^{202}Bi	^{201}Bi
1	246.5 ± 1.2	111.7 ± 0.3	78.4 ± 0.8	46.77 ± 0.18	32.5 ± 0.3	20.17 ± 0.21	10.6 ± 0.4
3	289.2 ± 1.2						
5	293.6 ± 1.5						
7	295.1 ± 1.3						
9	269.3 ± 1.5	138.3 ± 0.7	109.4 ± 1.3	71.1 ± 0.3	52.2 ± 0.5	37.2 ± 0.4	20 ± 0.5
11	255.1 ± 1.1						
13	232.3 ± 1.2						
15	211.4 ± 0.8						
17	186 ± 1.0						
19	167.5 ± 0.7						
21	148.6 ± 0.8	92.1 ± 0.5	77.7 ± 0.9	53.62 ± 0.23	42.8 ± 0.3	32.7 ± 0.4	19.2 ± 0.6
23	135.6 ± 0.6						
25	112.7 ± 0.8						
27	99.5 ± 0.5						
29	79.4 ± 0.5						
31	57.81 ± 0.29	54.4 ± 0.3	68.6 ± 1.0	59.07 ± 0.25	50.3 ± 0.4	43.5 ± 0.4	22.2 ± 0.6
33	34.94 ± 0.26						
35	23.75 ± 0.17						
37	15.75 ± 0.15						
39	11.98 ± 0.12						
41	9.59 ± 0.10						
43	7.92 ± 0.09	6.64 ± 0.05	5.74 ± 0.13	3.897 ± 0.026	3.36 ± 0.05	2.82 ± 0.08	1.78 ± 0.17
45	6.80 ± 0.09						

Table 3. Experimental reaction rates in iodine samples. Reaction rates $B(A)$ are multiplied with 10^8

9th cm	^{127}I	^{129}I	21st cm	^{127}I	^{129}I
^{130}I		259.3 ± 0.4	^{130}I		348.6 ± 0.5
^{128}I	344.4 ± 1.6	154.6 ± 1.6	^{128}I	216.9 ± 1.2	245 ± 3
^{126}I	284.1 ± 0.8	109.7 ± 2.3	^{126}I	157.1 ± 0.4	155.2 ± 2.1
^{124}I	76.6 ± 0.4	38 ± 3	^{124}I	48.1 ± 0.3	51 ± 4
^{123}I	59.27 ± 0.23	31.52 ± 0.22	^{123}I	46.42 ± 0.17	36.3 ± 0.4
^{121}I	16.8 ± 0.10	9.03 ± 0.14	^{121}I	14.03 ± 0.07	8.71 ± 0.19
^{120}I	9.43 ± 0.18	8.9 ± 2.1	^{120}I	9.7 ± 0.17	7 ± 4
^{119}I	4.24 ± 0.11	2.33 ± 0.23	^{119}I	4.4 ± 0.10	2.4 ± 0.5
^{118}I	1.35 ± 0.07		^{118}I	1.69 ± 0.06	

The codes successfully predict the general trends of the results and with some exceptions (which could be the systematical error) also the absolute values. The differences between the codes are minimal in the prediction of the production isotopes with lower threshold, but they become significant for some isotopes with threshold above 30 MeV. From the comparison with experimental data, it seems that the FLUKA code describes the neutron/proton spectrum after the 10th cm better than models included in MCNPX. Concerning the total number of produced neutrons in the setup, the calculations by various codes are in good agreement and predict 11.7–12.6 neutrons per one primary proton.

REFERENCES

1. *Van der Meer K. et al.* // Nucl. Instr. Meth. Phys. Res. B. 2004. V. 217. P. 202.

2. *Yurevich V. I. et al.* // Nucl. Instr. Meth. Phys. Res. A. 2006. V. 562. P. 747–749.

3. Group X-6, MCNPX 2.3.0 — Monte Carlo *N*-Particle Transport Code System for Multiparticle and High Energy Applications. LANL, Los Alamos, New Mexico, 2002.

4. *Fasso A. et al.* CERN-2005-10 2005; INFN/TC 05/11, SLAC-R-773.

5. *Majerle M. et al.* // Proc. of XVII ISHEPP. 2005. V. II. P. 135–140.

6. *Henzl V. et al.* // J. Nucl. Sci. Tech. Supplement 2. August 2001. P 1248.

7. *Krasa A. et al.* JINR Preprint E1-2005-46. Dubna, 2005.

8. EXFOR: Experimental Nuclear Reaction Data (EXFOR/CSISRS).

9. ICRU (1993). International Commission on Radiation Units and Measurements. ICRU Report 49. Stopping Powers and Ranges for Protons and Alpha Particles.

10. *Hendricks J. et al.* MCNPX, version 2.6.f, LA-UR-08-1808.

11. *Mashnik S. G. et al.* // J. Nucl. Radiochem. Sci. 2005. V. 6, No. 2. P. A1–A19.

12. *Mashnik S. G. et al.* // J. Phys. Conf. Ser. 2006. V. 41. P. 340–351.

13. *Junghans A. R. et al.* **//** Nucl. Phys. A. 1998. V. 629. P. 635.

14. *Chadwick M. B. et al.* **//** Nucl. Sci. Eng. 1999. V. 131, No. 3. P. 293.

15. *Ferrari A., Sala P. R.* **//** Proc. MC93 Int. Conf. on Monte Carlo Simulation in High Energy and Nuclear Physics, Tallahassee (Florida), 22–26 February 1993 / Ed. by P. Dragovitsch, S. L. Linn, M. Burbank. Singapore: World Scientific, 1994. P. 277–288.

16. *Koning A. J., Hilaire S., Duijvestijn M. C.* TALYS-1.0 **//** Proc. of the Intern. Conf. on Nuclear Data for Science and Technology — ND2007, April 22–27, 2007, Nice, France, 2008.

Корректор *Т. Е. Попеко*